Submitted to the International Europhysics Conference on High Energy Physics HEP99,
Tampere, Finland, July 1999

# Measurements of Transverse Energy Flow in Deep-Inelastic Scattering at HERA

H1 Collaboration

**Abstract**

Measurements of transverse energy flow are presented for neutral current deep-inelastic scattering events produced in positron-proton collisions at HERA. The kinematic range covers squared momentum transfers $Q^2$ from $3.2$ to $2\,200$ GeV$^2$, the Bjorken scaling variable $x$ from $8 \cdot 10^{-5}$ to $0.11$ and the hadronic mass $W$ from $66$ to $233$ GeV. The transverse energy flow is measured in the hadronic centre of mass frame and is studied as a function of $Q^2$, $x$, $W$ and pseudorapidity. A comparison is made with QCD based models. The behaviour of the mean transverse energy in the central pseudorapidity region and an interval corresponding to the photon fragmentation region are analysed as a function of $Q^2$ and $W$.

**Abstract: 157l**
**Parallel sessions: 3**
**Plenary sessions: 3**

# 1 Introduction

Measurements of hadronic final state quantities are extremely useful in investigating the different QCD processes that occur in the wide range of phase space made accessible by the $ep$ collider HERA. One such quantity is transverse energy, measurements of which contain global information about charged and neutral particles and cover a wider pseudorapidity range than equivalent available charged track analyses [1, 2, 3].

Electron-proton scattering for values of $Q^2$, the virtuality of the exchanged boson, significantly above $1$ GeV$^2$ is usually considered as a deep inelastic scattering (DIS) process, in which an exchanged boson directly couples to a parton in the proton. This approach successfully describes inclusive cross-section measurements [4, 5], provided that appropriate parton distribution functions are used to describe the partonic content of the proton. Several approaches, based on the DGLAP [6], BFKL [7] and CCFM [8] equations are available for the QCD evolution of these parton densities to an appropriate scale before the interaction with the exchanged boson.

Extending this picture to describe the hadronic final state introduces a number of further complications. It becomes not only necessary to understand what happens to the parton involved in the partonic scattering process in more detail, but also to understand the effects of the interaction on the entire proton. Thus the influence of the evolution process leading to the parton undergoing the hard scattering must be modelled, as must the behaviour of the proton remnant and the fragmentation process. Measurements of transverse energy flow [3, 9] have proven useful in discriminating between the different approaches used in these QCD models. For example, it was shown that early Monte Carlo models based on DGLAP evolution tended to produce insufficient transverse energy in the region near the proton remnant for values of the Bjorken scaling variable $x$ of less than about $10^{-3}$.

Recent measurements of jet and leading particle production in DIS [10, 11, 12] suggest that the description of the data provided by DGLAP based models can be improved by allowing the virtual photon to have structure. That is, in addition to "direct photon" events, in which the entire momentum of the virtual photon enters the hard scattering process, "resolved photon" events are allowed. In these, the virtual photon is considered to have a developed partonic structure and one of the partons in the photon participates in the hard interaction. The significance of this idea for the description of the transverse energy flow, in the framework of the above models of DIS, is also investigated in this paper.

The deep inelastic $ep$ scattering may also be viewed in the rest frame of the proton. In this frame the photon can be considered to fluctuate into a hadronic object which subsequently interacts with the proton, even for $Q^2$ values of up to $1\,000$ GeV$^2$ [13, 14, 15]. In the proton rest frame and for values of $Q^2$ above several GeV$^2$ the fluctuation time [16, 14] is given by $\tau \approx 1/(xM_p)$, where $M_p$ is the mass of the hadronic target. For values of $x$ of less than $10^{-2}$ the virtual photon can fluctuate into and exist as a hadronic object over a distance of $10$ to $1\,000$ fm, which is far larger than the size of the proton. Under the naïve assumption that this fluctuation behaves like a single hadron then $ep$ interactions should resemble hadron-hadron scattering. This approach was tested in an earlier publication [17], in which it was demonstrated that the average transverse energy flow in the central rapidity region in the hadronic centre of mass system showed no significant $Q^2$ dependence. This is consistent with observations made in hadron-hadron scattering, in which particle production in the central region is largely independent of the nature of the hadronic object and depends only on the total centre of mass energy [18]. Conversely, transverse energy production in the expected photon fragmentation region was found to be strongly dependent on $Q^2$. The data collected by H1 in recent years now allow this picture to be studied with far greater precision than was possible in the previous work [17].

It is the aim of this analysis to study transverse energy production within both the traditional DIS framework and in the picture given in the proton rest frame. Distributions showing the dependence of transverse energy on pseudorapidity, $x$, $Q^2$ and the total hadronic mass, $W$, are presented and quantitative comparisons of QCD based models are made with the data. A more qualitative approach is adopted in examining the interpretation of our data as a hadron-hadron scattering process. The $Q^2$ and $W$ dependence of transverse energy production in the central pseudorapidity region and a region associated with the fragmenting photon is investigated and compared to hadron-hadron data and earlier H1 results in both photoproduction and DIS.

The analysis presented here is based on data taken at the HERA collider for which $820$ GeV protons were collided with $27.5$ GeV positrons at a centre of mass energy of $300$ GeV. Transverse energy production in the hadronic centre of mass system is studied in the kinematic range $3.2$ GeV$^2$ $< Q^2 <$ $2\,200$ GeV$^2$, $x > 8 \cdot 10^{-5}$ and $66 < W < 233$ GeV. An order of magnitude more data are used than in the previous H1 measurements [9, 17]. Furthermore, the phase space region has been extended into the proton remnant fragmentation region and now covers more than 8 units of pseudorapidity.

## 2 The H1 Detector

A detailed description of the H1 apparatus can be found elsewhere [19]. The following section briefly describes the components of the detector relevant to this analysis.

The H1 liquid argon (LAr) calorimeter [20] was used to measure positrons scattered into the central and forward (proton direction) parts of the H1 detector and also to determine the hadronic energy flow. The calorimeter extends over the polar angle range $4^\circ < \theta < 154^\circ$ with full azimuthal coverage, where $\theta$ is defined with respect to the incoming proton direction. It consists of an electromagnetic section with lead absorbers and a hadronic section with steel absorbers. Both sections are highly segmented in the transverse and longitudinal directions. Energy resolutions for electrons [21] and charged pions [22] of $\sigma_{E_e}/E_e \approx 0.12/\sqrt{E_e\,[\text{GeV}]} \oplus 0.01$ and $\sigma_{E_h}/E_h \approx 0.50/\sqrt{E_h\,[\text{GeV}]} \oplus 0.02$, respectively, have been established in test beams. The uncertainties in the absolute electromagnetic and hadronic energy scales are $3\%$ and $4\%$, respectively, for the present data sample.

The backward electromagnetic lead-scintillator calorimeter (BEMC) was used to measure the properties of the scattered positron for polar angles in the range $155^\circ < \theta < 176^\circ$. An energy resolution of $0.10/\sqrt{E_e[\text{GeV}]} \oplus 0.42/E_e[\text{GeV}] \oplus 0.03$ has been achieved [23]. The absolute electromagnetic scale has been determined to a precision of $1\%$ [24]. Since it consists of only one interaction length of material, the hadronic response of the BEMC is poor and approximately 30% of incident hadrons leave no significant energy deposition. Consequently, a large scale uncertainty of 20% exists for hadronic measurements made with this device. For results presented here based on 1994 data, the BEMC was used both to measure properties of the scattered positron and the hadronic energy flow.

The BEMC was replaced in 1995 by the SPACAL as the main rear calorimeter in the H1 detector. This contains electromagnetic and hadronic sections, achieving energy resolutions of $0.075/\sqrt{E_e\,[\mathrm{GeV}]} \oplus 0.025$ and $30\%$ for positrons and hadrons, respectively [25]. The absolute electromagnetic energy scale is known to a precision of $2\%$ and the hadronic energy scale to $7\%$ [26]. For the analysis presented here, the SPACAL is used to measure hadronic energy flow for events in which the scattered positron is reconstructed in the LAr.

A series of tracking chambers are in place which provide the measurement of the polar angle of the scattered positron in this analysis. Forward and central tracking chambers cover polar angle ranges of $5^\circ < \theta < 25^\circ$ and $25^\circ < \theta < 155^\circ$, respectively, and provide a measurement of the primary vertex position and the polar angle of the scattered positron. In the backward region ($155^\circ < \theta < 176^\circ$) the scattered positron is measured by the Backward Proportional Chamber (BPC) which lies in front of the BEMC. These detectors allow the polar angle of the scattered positron to be measured with a precision of $1$ mrad [4].

The transverse energy flow measurement is extended in the proton direction by a small calorimeter (PLUG) with copper absorber and silicon pad readout, covering the region between the beam-pipe and the LAr cryostat ($0.7^\circ < \theta < 3.3^\circ$). Owing to the large amount of passive material between the PLUG and the interaction point, which varies between $0.8$ and $5$ interaction lengths, less than $40\%$ of the energy measured in the PLUG originates from the primary vertex. Using a full simulation of the material distribution in and around the H1 detector, energy loss corrections have been determined. The precision of these corrections has been studied using $ep$ data [27]. An energy scale uncertainty of 26% and an energy resolution of $1.5/\sqrt{E_h\,[\mathrm{GeV}]}$ have been achieved.

# 3 Event Selection

In this analysis three independent event samples are considered: two from the 1994 and one from the 1996 data taking period. The 1994 low $Q^2$ samples consist of events in which a scattered positron is found in the BEMC and correspond to running periods in which the $ep$ interaction point was at the nominal position and in which it was shifted by about 67 cm in the proton direction, $z$. This shift allowed lower $Q^2$ values, down to 2.5 GeV$^2$, to be accessed. The 1994 data samples together permit the range $2.5$ GeV$^2$ $< Q^2 < 100$ GeV$^2$ to be studied. The integrated luminosities of the nominal and shifted vertex data samples are $2.7$ pb$^{-1}$ and $0.058$ pb$^{-1}$, respectively.

The high $Q^2$ sample consists of events collected in 1996 and corresponds to an integrated luminosity of $8.2$ pb$^{-1}$. For this sample, the scattered positron is detected in the LAr calorimeter and $Q^2$ is required to be larger than $100$ GeV$^2$.

DIS events are selected by demanding a well-reconstructed scattered positron with an energy larger than $12$ GeV. The event kinematics are determined using the scattered positron energy, $E'_e$, and polar angle, $\theta_e$ (electron method): $Q^2 = 4E_eE'_e\ \cos^2(\theta_e/2)$ and $y_e = 1 - (E'_e/E_e)\ \sin^2(\theta_e/2)$ where $E_e$ is the incident positron beam energy. The scaling variable Bjorken-$x$ is related to these quantities via the square of the centre of mass energy $s$: $x = Q^2/(ys)$, and the hadronic invariant mass squared is $W^2 = sy - Q^2$.

In addition, the following selection criteria are applied to suppress non-$ep$ and photoproduction background and to maintain optimal resolution in the kinematic variables:

- A reconstructed event vertex must be found within $\pm 30$ cm in $z$ of the nominal interaction point.
- The longitudinal momentum balance must be within $30$ GeV $< \sum_i E_i - P_{zi} <$ $70$ GeV, where the sum runs over all energy deposits in the LAr and the backward calorimeter.
- $W_e^2$, the invariant mass squared of the hadronic final state determined using the scattered positron is required to be larger than $4\,400\,\mathrm{GeV}^2$.
- The invariant mass of the hadronic final state determined using the hadronic energy deposited in the calorimeters, $W_h$, is also required to satisfy $W_h^2 > 4\,400\,\mathrm{GeV}^2$.
- To reduce background from photoproduction interactions, $y_e < 0.6$ is required.

For the low $Q^2$ sample the positron candidate is required to be found within the angular acceptance of the BEMC ($157° < \theta_e < 173°$ for the nominal vertex data and $164° < \theta_e < 176°$ for the shifted vertex data). In addition, positron identification cuts to suppress photoproduction background are made using the information obtained from the BEMC cluster radius and the matching of the cluster position with that of a charged particle measured in the BPC.

For the high $Q^2$ sample the scattered positron candidate is required to be found within the LAr calorimeter ($\theta_e < 150°$). Since the high $Q^2$ analysis is especially sensitive to QED radiation collinear with the $e^+$ beam, further selection criteria are included:

- $0.5 < y_h/y_e < 1.3$. The variable $y_h$ is given by the Jacquet Blondel method [28]: $y_h = \frac{1}{2}\Sigma/E_e$ where $\Sigma = \sum_i(E_i - p_{zi})$ and $i$ refers to all energy clusters detected in the calorimeters except that due to the scattered positron.
- In addition to the electron method, the $\Sigma$ method [29] is used to calculate $x$ and $Q^2$ and a requirement is made that both methods should prescribe the same kinematic bin for a given event. According to the $\Sigma$ method $Q^2$ , $y$ and $x$ are given by
  $Q^2_\Sigma = {E'_e}^2 \sin^2\theta_e/(1-y_\Sigma)$, $y_\Sigma = \Sigma/(\Sigma + E'_e(1-\cos\theta_e))$ and $x_\Sigma = Q^2_\Sigma/(sy_\Sigma)$.

After the application of these cuts, the efficiency for selecting events for every interval in $x$ and $Q^2$ used in this study is greater than 75%.

The high $Q^2$ data from 1994 have also been studied. The transverse energy flow measurements made with the two high $Q^2$ data sets are consistent within their statistical errors. Because of the different correction procedures necessary for the 1994 and the 1996 data samples and the significantly larger amount of data available to the 1996 high $Q^2$ analysis, the two measurements have not been combined and for the high $Q^2$ region only results based on 1996 data are presented here.

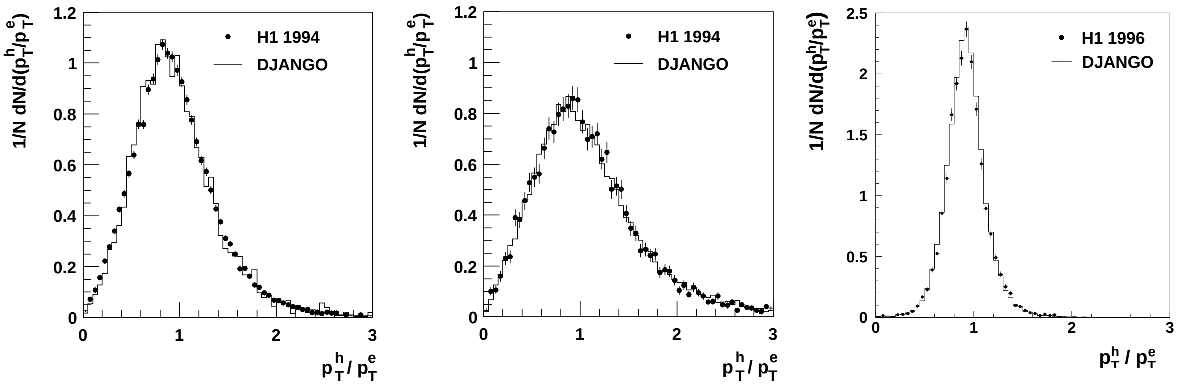


Figure 1: The distribution of $p_T^h/p_T^e$ measured with the 1994 nominal vertex data-set (left), the 1994 shifted vertex data-set (middle) and the 1996 data-set (right). The data are compared with predictions from DJANGO.

# 4 Experimental Method

The data are corrected bin-by-bin for QED radiation and detector effects using the event generator DJANGO [30] together with a full simulation of the detector response. To demonstrate the accuracy of the simulation and the understanding of the response of the H1 calorimeters the distributions of transverse momentum balance, $p_T^h/p_T^e$, are shown in Fig. 1 for the different data samples used in this analysis. Here, $p_T^h$ is defined as the sum of the azimuthal four-momentum vector components $x$ and $y$ of each energy deposition $i$ in the LAr and SPACAL calorimeters according to $(p_T^h)^2 = (\Sigma_i p_{x,i})^2 + (\Sigma_i p_{y,i})^2$. Similarly, $p_T^e$ is the transverse momentum of the scattered positron. Predictions made with the DJANGO model are also shown and they describe the data well.

The work presented in this paper comprises studies of the production of transverse energy $E_T^*$ as a function of pseudorapidity $\eta^*$ and the kinematics of the $ep$ scattering process. Measurements are made of the distribution $1/N dE_T^*/d\eta^*$ in which, for a specified kinematic range, $N$ is the total number of DIS events and $dE_T^*/d\eta^*$ is the sum of the transverse energies of each particle $i$ per unit of pseudorapidity. The transverse energy, $E_{Ti}^*$, of a particle $i$ with energy $E_i^*$ and polar angle $\theta_i^*$ is defined as $E_{Ti}^* = E_i^* \sin\theta_i^*$. Results are given in the hadronic centre of mass system (hCMS) for which the incoming photon direction defines the $+z^*$ direction.[1]

Whereas in the laboratory frame (LAB) a sizeable contribution to the transverse energy is produced by the kinematic recoil from the scattered lepton, in the hCMS transverse energy is due largely to perturbative QCD and fragmentation effects. The Lorentz transformation from the LAB into the hCMS therefore serves to isolate the physically interesting part of the $E_T$ flow.

At high $Q^2$ the Lorentz transformation from the LAB to the hCMS requires great care. Any deviation from the true transformation produces an artificial contribution to the transverse energy seen in the hCMS. This is a more severe problem at high $Q^2$ than at low $Q^2$ since the mean particle transverse energy increases with $Q$ in the LAB but depends only weakly on $Q$ in the hCMS. For the high $Q^2$ data sample the maximum $\langle E_T\rangle$ per unit pseudorapidity is

[1] All quantities presented in the hCMS frame are denoted by the superscript *

typically an order of magnitude larger in the LAB than in the hCMS (about 20 GeV compared to 2 GeV). In practice the transformation is calculated from the energy and direction of the scattered positron. The main sources of error are the energy resolution and calibration of the calorimeters and QED radiation. Although the energy resolution and calibration of the H1 LAr calorimeter are well understood and the influence of QED radiation is well described by DJANGO, these remain an important source of systematic bias. To minimise their influence on the measurement of the transverse energy for the high $Q^2$ data, the method described below was used. This exploits the precise information which is available on the direction of the scattered lepton.

A deviation in the energy measurement of the scattered positron results in an artificial component in the momentum of any particle in the hCMS which lies within the scattering plane defined by the incoming proton and the scattered positron. To suppress this artificial momentum, the variable used to measure transverse energy in the high $Q^2$ data set is redefined as $E^*_\perp = E^*_T|\sin\varphi^*|\frac{\pi}{2}$, where $\varphi^*$ is the azimuthal angle w.r.t. the lepton scattering plane. Integrated over $\varphi^*$ this is again equal to $E^*_T$, assuming an isotropic distribution of the true transverse energy around the proton in the hCMS in $\varphi^*$. Therefore the measurements of $\langle E^*_T\rangle$ and $\langle E^*_\perp\rangle$ are equivalent for an isotropic $\varphi^*$ distribution. Although $\varphi^*$ asymmetries are predicted in pQCD from processes such as boson-gluon fusion and QCD-Compton scattering they introduce biases of less than 1% in the transverse energy flow at high $Q^2$. This is a significantly smaller effect than the biases due to poor $E^*_T$ resolution which would be introduced were the redefinition not used.

# 5 Systematic Errors

There are several sources of systematic effects which may affect the measurements presented in this paper. The systematic errors owing to these have been investigated [27, 31] and are discussed below.

- The hadronic energy scales of the calorimeters are known to an accuracy of $4\%$ (LAr), $26\%$ (PLUG), $7\%$ (SPACAL) and $20\%$ (BEMC). This directly gives the uncertainties for the energy measurements presented here.
- For the scattered positron the energy calibration uncertainty is $1\%$ in the BEMC region (low $Q^2$ sample) and $3\%$ for the LAr calorimeter (high $Q^2$ sample). Resulting errors on measured $E^*_T$ are typically $2\%$ at low $Q^2$ and $6\%$ at high $Q^2$ . At high $Q^2$ and at large values of $\eta^*$ this error can become large ($\leq 27\%$). Section 7.1 describes in more detail the specific problems related to the high $Q^2$ measurements.
- Uncertainties owing to the reconstruction of the kinematic variables $x$ and $Q^2$ are typically of the order of $2\%$ and $1.5\%$ for the low $Q^2$ and high $Q^2$ spectra, respectively. The improved precision at high $Q^2$ is due to the additional cuts applied to this data sample (see section 3).

- The model dependence of the bin-by-bin correction is estimated using the event generators ARIADNE [32], HERWIG [33] and LEPTO [34] with two parton density functions (GRV [35] and MRSH [36]). The differences between the models are typically $3\%$ at high $Q^2$ and $4.5\%$ at low $Q^2$. Larger differences are found for the two $\eta^*$ bins measured with the PLUG calorimeter ($20\%$). The larger errors in the PLUG pseudorapidity region are due to the uncertainties in the modelling of the physics in this region.

- The transverse energy measurement is strongly reliant on a correct simulation of the inactive material in and around the H1 detector, particularly in the forward region. The sensitivity of the measurements to the assumed material distribution is estimated by varying the amount and location of the inactive material in the simulation. The transverse energy flows measured with the 1994 and 1996 data, for which different configurations of dead material were present, are also compared. This gives rise to typical uncertainties of the order of $4\%$ for the data samples. These differences are included as systematic errors. For the points measured with the PLUG calorimeter a different procedure is used. Using the shifted vertex and the nominal vertex data sets energy flow is measured in approximately the same detector volume in the PLUG although incident particles pass through different amounts of inactive material. After applying the dead material correction, the change in total energy measured in the PLUG is compatible with Monte Carlo expectations to within $5\%$. The magnitude of the total energy shift observed in data between the nominal and shifted vertex event samples, $11\%$, is taken as the systematic error on this measurement due to the influence of dead material.

- Another possible source of error is the simulation of the hadronic shower within the LAr and the PLUG calorimeters. This has been investigated by comparing the simulation programs GHEISHA [37] and CALOR [38]. The differences are small for the LAr calorimeter ($3\%$) but large for the PLUG calorimeter ($20\%$).

- Photoproduction background is only important at low $Q^2$. The typical uncertainty on the measured points owing to this source is $1\%$ and has been estimated with the PHOJET [39] program.

# 6 QCD-based Models

Although progress has been made on several other fronts [40, 41, 42, 43] it is still the case that most QCD based predictions of the hadronic final state are produced with Monte Carlo methods which use the following prescription. Phenomenologically derived parton distribution functions, evolved to the relevant scale, are used to determine the properties of the partons emerging from the initial state hadron, or photon. Some of these partons undergo a hard scatter, the cross-section for which is calculated using leading order (LO) QCD. The resulting partons undergo fragmentation to produce the observed hadrons.

The proton parton distribution functions are reasonably well constrained by inclusive measurements of DIS (in particular $F_2$), and data from hadron-hadron scattering experiments. The effects on the hadronic final state of changing the input parton distribution functions within the limits allowed by the inclusive DIS data are small compared to the effects arising from varying other aspects of the calculations. The proton parton distribution functions used here are the CTEQ4L [44, 45] set. For calculations involving resolved virtual photon processes, the SAS-G virtual photon parton parameterisation [46] is used.

Different QCD evolution equations are known. They have been derived in the Leading-Log-Approximation and are expected to be valid in certain regions of Bjorken $x$. The DGLAP evolution equation effectively resums the leading $\log Q^2$ terms which corresponds to the strong ordering in transverse momentum of successive parton emissions and is applicable at large $Q^2$. The BFKL approach sums leading $\log(1/x)$ terms and is expected to become significant at small $x$. Successive parton emissions in this approach have strongly decreasing longitudinal momenta, but are not ordered in transverse momentum. This latter feature is emulated in parton emissions produced by the Colour Dipole Model (CDM) [47] in which partons are radiated from colour dipoles produced in the hard interaction [48]. The CCFM evolution equation forms a bridge between the DGLAP and BFKL approaches and resums the leading $\log 1/x$ and $\log Q^2$ terms both for inclusive and non-inclusive quantities. To obtain CCFM based hadronic final state predictions, the Linked Dipole Chain [49] model is used here. This is a reformulation of the CCFM equation and redefines the separation of initial and final state QCD emission using the CDM.

The fragmentation of the produced partons typically involves a showering process followed by a hadronisation phase. The models to which the data are compared here use the string [50] or cluster [51] approach to hadronisation.

Although the evolution equations discussed above can be derived within the picture of a parton cascade, neither the DGLAP nor BFKL approximations describe the details of the hadronic final state. It is therefore necessary to reformulate these inclusive equations as an iterative process, the shower algorithm, to produce parton emissions in the Monte Carlo models.[2] The amount of transverse energy depends on these shower algorithms and hence the expected levels of $E_T$ are sensitive to the different evolution schemes.

The Monte Carlo models used here are based on various combinations of the above ideas. They are described briefly in the following text as are any changes to the default settings and modifications of the Monte Carlo programs.

ARIADNE [32] version 4.10. This is an implementation of the CDM. In order to generate an increase of the transverse energy with $Q^2$ the program has been modified; an additional switch has been introduced [52] and is set to MHAR(151)=2. This changes the phase space restriction for radiation from an extended source. In addition, two control parameters were changed from their default values. The parameter settings used are PARA(10)=1.5 and PARA(15)=0.5 [53]. These alter the suppression of radiation from the proton remnant and the struck quark, respectively. The expectations of this model are marked “ARIADNE 4.10 mod” on all figures.

The LDCMC [54], version 1.0. This is based on the Linked Dipole Chain implementation of CCFM evolution and uses the CDM to simulate the effect of higher order emissions. It is incorporated in the framework of the ARIADNE package. All parameters used by both programs are set to their default values, with the exception of those listed above. The expectations of this model are marked “LDCMC” on all figures.

[2]The CCFM approach is an iterative process by definition.

LEPTO 6.51 [34]. LEPTO matches exact first order QCD matrix elements to DGLAP based leading log parton showers. It also allows two different methods of non-perturbative rearrangement of the event colour topology. One way is via "soft colour interactions" (SCI) [55], in which low momentum gluons are exchanged between partons in the proton remnant and those which are perturbatively produced and this is the default option for this version of LEPTO. However, this scheme leads to an excess of soft particle production at high $Q^2$ [56]. In a different approach, a string reinteraction scheme based on a Generalised Area Law (GAL) is now available [57]. This allows interactions between the colour strings connecting the final state partons, leading to a reduction in the total string area. To use this option, retuned values of parameters relating to the hadronisation and the parton shower schemes have to be used.[3] However, as is demonstrated later in this report, the implementation of this scheme leads to a worsening of the description of our data. Because of this, the GAL option is not used in comparisons with most of the spectra presented here and model expectations which use neither GAL nor SCI are marked "LEPTO 6.51 mod" on these figures.

RAPGAP 2.06/48 [58]. RAPGAP also matches exact first order QCD matrix elements to DGLAP based leading log parton showers. In addition to the direct photon processes simulated by LEPTO, RAPGAP simulates resolved photon interactions in which the virtual photon is assumed to have structure, parameterised using an implementation of the SAS-G virtual photon parton distributions. The RAPGAP package allows a choice of renormalisation and factorisation scales. For predictions presented here, these are set to $p_T^2 + Q^2$, where $p_T$ is the transverse momentum of the partons in the hard scattering. The default value for the cut-off necessary to regulate the matrix elements is $p_T^2 > \mathrm{PT2CUT} = 1.0\,\mathrm{GeV}^2$. This leads to a predicted DIS cross-section which is larger than measurements for $Q^2 > 200\,\mathrm{GeV}^2$, so here $\mathrm{PT2CUT} = 4.0\,\mathrm{GeV}^2$ is used. The expectations of this model are marked "RAPGAP 2.06/48 dir + res" on all figures. If only direct photon interactions are allowed, the results of RAPGAP are very similar to those of LEPTO.

To perform the hadronisation step, all of the above models use string fragmentation as implemented in JETSET 7.4 [59].

HERWIG 5.9 [33]. This model is based on leading log parton showers with matrix element corrections [60] and implements a cluster hadronisation scheme. The expectations of this model are marked "HERWIG 5.9" where shown.

The PHOJET [39] Monte Carlo program is used to calculate the amount of background due to photoproduction processes. This generator contains LO QCD matrix elements for hard subprocesses, a parton shower model and a phenomenological description of soft processes.

As an alternative to the Monte Carlo based approach, analytical BFKL calculations [61] are available to predict energy flow in the forward region. These calculations are based on asymptotic expressions derived from the BFKL equation at LO and do not include hadronisation effects. The predictions of the calculations are marked "BFKL Partons" where shown.

[3]The following parameter settings are used with the GAL string re-interaction option: LST(34)=3, PARJ(42)=0.45, PARJ(82)=2.0, PYPAR(22)=4.0, and PARL(7)=0.10

# 7 Results

## 7.1 Transverse Energy

In addition to the selection criteria outlined in section 3, a further cut on the total energy produced in the angular region $4.4° < \theta < 15°$ is also imposed. The energy in this angular region is required to be larger than $0.5$ GeV ($E_{fwd}$ cut). This condition was introduced for the low $Q^2$ analysis to suppress diffractive-like events, which are characterised by an absence of hadronic energy in the forward region [62, 63]. It allows a comparison with the predictions of QCD based models which is less dependent on uncertainties introduced by the attempt to model diffractive processes.

In Fig. 2 the $E_T$ flow in the hCMS is presented in 17 regions of low $Q^2$ and $x$. The values of average $Q^2$ cover a range from $3.2$ GeV$^2$ to $70$ GeV$^2$ and the mean values of $x$ extend from $0.08 \cdot 10^{-3}$ to $7 \cdot 10^{-3}$. Here, and in all following figures in which two sets of error bars are displayed, the total errors (outer error bars) are the result of adding in quadrature the statistical errors (inner error bars) and the systematic errors.

The data exhibit a mean transverse energy of approximately $2$ GeV per unit of pseudorapidity. The $E_T$ flow shows a plateau for $Q^2$ values below about $10$ GeV$^2$ in the current region ($\eta^* > 0$), although as $Q^2$ increases the distributions become peaked in this region. Using the PLUG calorimeter it is possible to measure transverse energy in the vicinity of the proton remnant; these data can be seen as the two points at smallest $\eta^*$. Here the transverse energy flow tends to be about one half of that which is measured in the current region.

The systematic errors on the $E_T^*$ measurements shown in Fig. 2 are correlated. The measurements in the range $-1 < \eta^* < -4$ were made predominantly using the LAr calorimeter and suffer from a 10% normalisation uncertainty owing to the LAr hadronic energy scale and the model dependence of the correction procedure. These are uncorrelated with the errors on the measurements made using the PLUG and the BEMC calorimeters. For each $x$ and $Q^2$ interval the PLUG was used exclusively for the data points at the two lowest values of $\eta^*$ and the BEMC was the main calorimeter used for measurements in three highest $\eta^*$ bins. The errors on the measurements provided by both of these calorimeters are predominantly normalisation uncertainties.

In Fig. 2 four QCD models, ARIADNE, HERWIG, LEPTO and RAPGAP are compared to the data. These models give an acceptable overall description of the measured transverse energy flow with the exceptions that HERWIG fails to describe the shape of the distribution for values of $Q^2$ above about 7 GeV$^2$ and shows a peak at $\eta^* \approx 1$ and LEPTO fails to match the data in the central pseudorapidity region for the lowest values of $x$ and $Q^2$. ARIADNE and RAPGAP give the best description of all of the models in the lowest $x$ and $Q^2$ bins although each tends to overestimate the transverse energy flow in the vicinity of the proton remnant.

The measurements at high $Q^2$ are shown in Fig. 3. The $E_T$ flow is presented in 7 regions in $x$ and $Q^2$ and compared again to the four QCD models. At high $Q^2$ the experimental resolution in $\eta^*$ becomes strongly dependent on $x$ and $Q^2$ and the $\eta^*$ bin widths are adjusted accordingly. The average $Q^2$ values cover a range from $175$ GeV$^2$ to $2\,200$ GeV$^2$ and average $x$ from 0.0043 to 0.11. For consistency with the low $Q^2$ results the $E_{fwd}$ cut is applied, although its influence

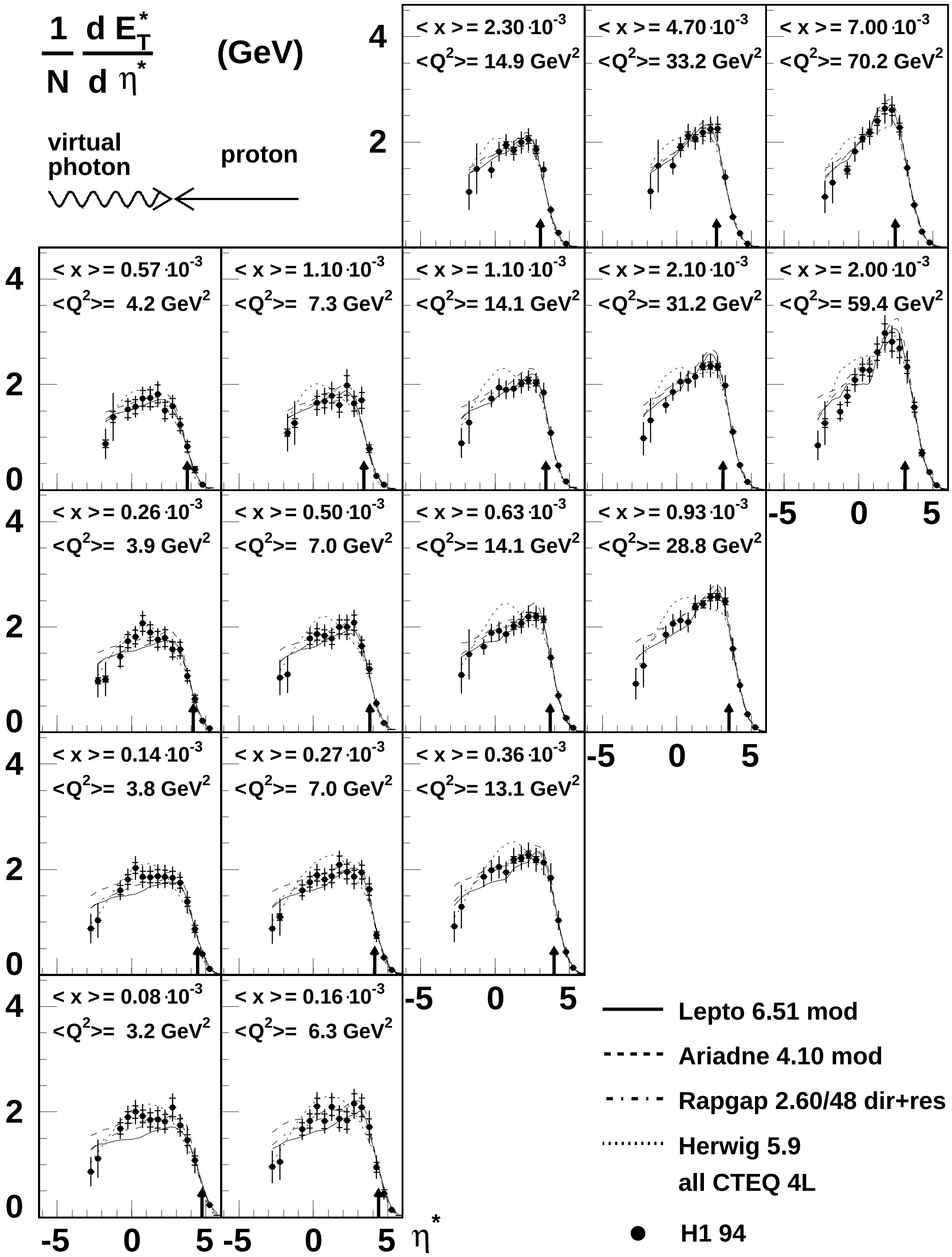


Figure 2: The inclusive transverse energy flow $1/N dE_T^*/d\eta^*$ at different values of $x$ and $Q^2$ for the low $Q^2$ sample. Note that the errors on all of the measurements made at the two lowest values of $\eta^*$ in each $x$ and $Q^2$ interval are highly correlated and largely independent of the errors at larger values of $\eta^*$. The data are compared to four QCD based models. The arrows mark the average position of the origin of the Breit frame ($\frac{1}{2}\ln\frac{1}{\langle x\rangle} - 1$).

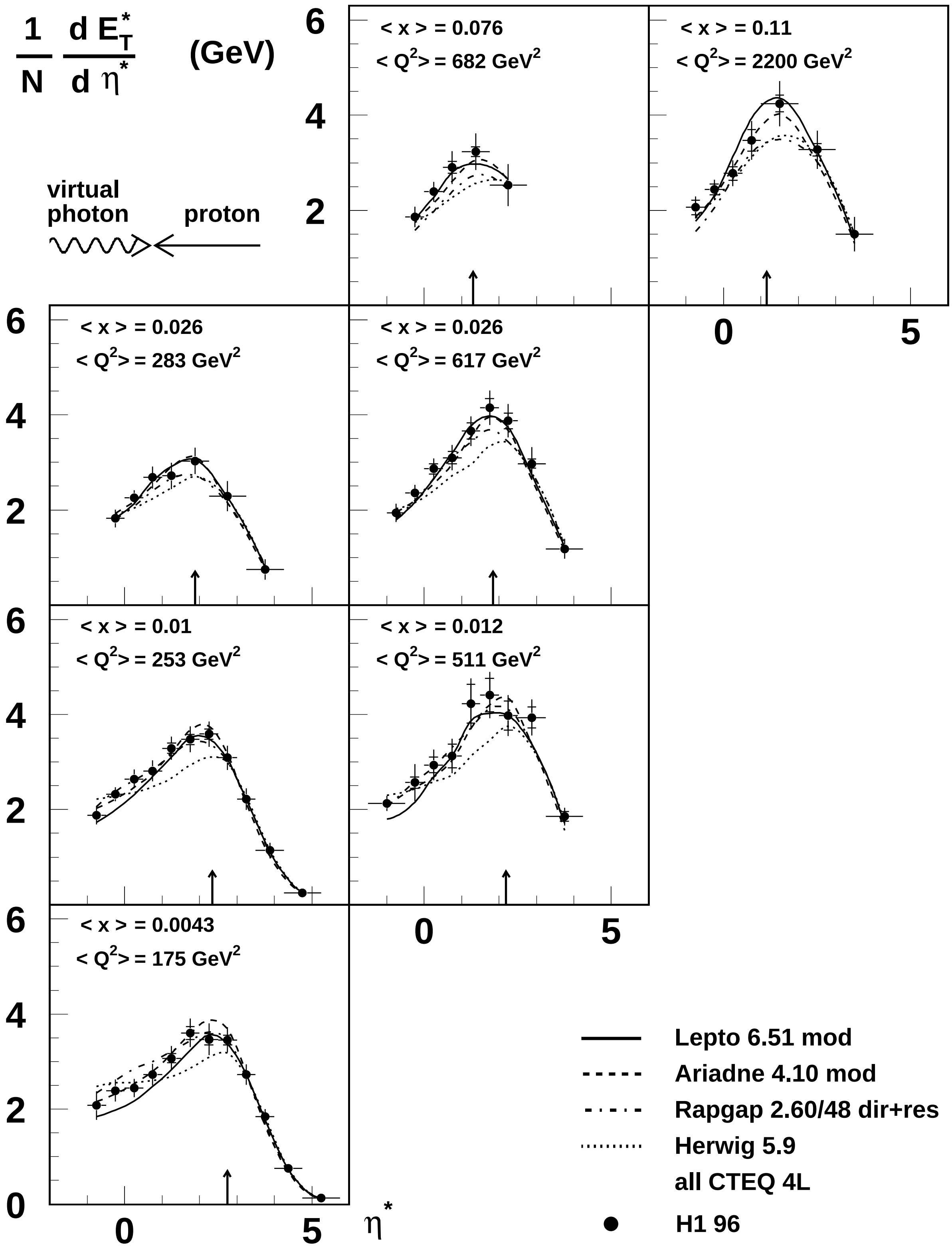


Figure 3: The inclusive transverse energy flow $1/N dE_T^*/d\eta^*$ at different values of $x$ and $Q^2$ for the high $Q^2$ sample. The data are compared to four QCD based models. The arrows mark the average position of the origin of the Breit frame ($\frac{1}{2}\ln\frac{1}{\langle x\rangle} - 1$).

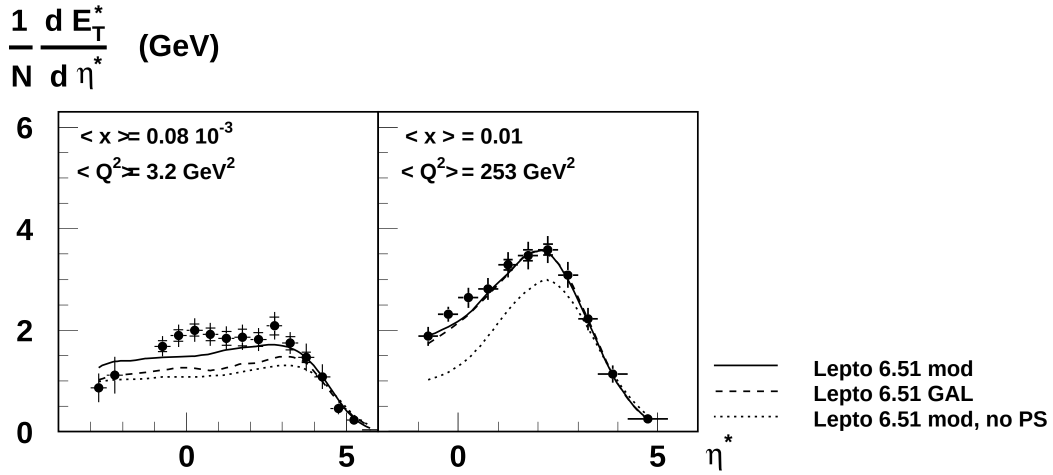


Figure 4: The inclusive transverse energy flow $1/NdE_T^*/d\eta^*$ for two selected kinematic bins from Figs. 2 and 3. The influence of GAL string reinteractions and parton showers on the expected transverse energy flow are shown.

is small at high $Q^2$. As is the case for the low $Q^2$ spectra, the transverse energy flow is seen to peak in the current region. Here, the measured transverse energy is significantly higher than at low $Q^2$ . In this kinematic range all QCD models describe the data well with the exception of HERWIG which produces insufficient transverse energy over the $Q^2$ range shown and does not describe the shape of the energy flows.

At high $Q^2$ the positions of the maxima of the $E_T$ flow coincide approximately with the average origin of the Breit frame at $\eta^*_{O-BF} = \frac{1}{2}\ln\frac{1}{\langle x\rangle} - 1$. The Breit frame (BF) is defined as the frame in which the exchanged boson carries the momentum $(0,0,0,-Q)$. In [64] it was argued that at high $Q^2$ the maximum of the radiated transverse energy should coincide with $\eta^*_{O-BF}$. This behaviour can be seen in our data. In Fig. 2 and Fig. 3 the position of $\eta^*_{O-BF}$ is marked by an arrow.

In Fig. 4 the transverse energy flow is shown for two $Q^2$ bins ($\langle Q^2\rangle = 3.2$ GeV$^2$ and $\langle Q^2\rangle = 253$ GeV$^2$) compared to the predictions of LEPTO with different parameter settings. The effects of using GAL based string reinteractions are shown as the dashed line. The solid line represents LEPTO predictions when the GAL model is not used. The GAL approach leads to a deficit of transverse energy production at low $Q^2$ although its effect is small at high $Q^2$. The expectations of LEPTO without parton showers (PS) are shown as the dotted curves. The predictions lie below the data for most of the pseudorapidity range measured, illustrating the sensitivity of our measurements to pQCD processes, as modelled here using a parton shower algorithm.

## 7.2 Dependence on Bjorken-$x$

It has so far proved impossible to distinguish between the different QCD evolution schemes mentioned in section 6 using inclusive structure function measurements. It has been suggested that the hadronic final state may prove to be a more sensitive testing ground [65]. Measurements of energy flow [9], jets and leading particles [12] in the region near the proton remnant have indicated that DGLAP parton evolution fails to produce sufficient QCD radiation at low $x$. On the other hand, BFKL evolution predicts a rise of hard parton emissions at low $x$ in the central pseudorapidity region of the hCMS.

To study these QCD evolution effects, the dependence of the mean transverse energy in the central pseudorapidity region ($-0.5 < \eta^* < 0.5$) with $x$ is shown in Fig. 5 for different ranges of $Q^2$. The central region has been chosen since it is less affected by the hard scattering and still lies within the acceptance of the H1 detector. A rise in the measured transverse energy is observed as $x$ decreases. The general behaviour of the data can be understood as a rise of the average transverse energy with hadronic mass, $W$, which increases as $x$ decreases at fixed $Q^2$.

The QCD based Monte Carlo models exhibit reasonable agreement with the data over most of the kinematic range presented here. However, the shape of the $x$ dependence as predicted by the DGLAP based model LEPTO does not follow closely the data at the smallest $Q^2$ and $x$ values shown in Fig. 5. The calculations of the CCFM based LDCMC show the same behaviour in this region. Analytical BFKL calculations at the parton level [61] describe the $x$ dependence better and are closer to the data at the lowest values of $Q^2$ and $x$. However, uncertainties due to hadronisation corrections and missing higher orders in the calculations preclude an interpretation of the data as a signal of the onset of BFKL dynamics.

The effects of a resolved component of the virtual photon provide another possible explanation of the observed increase of transverse energy production with decreasing $x$. Calculations using RAPGAP including resolved and direct virtual photon components describe well the $x$ dependence and the amount of transverse energy flow. The CDM approach of ARIADNE is also in good agreement with the data.

## 7.3 Dependence on $Q^2$ and $W$

As mentioned in the introduction, photon-proton scattering is similar to a hadron-hadron process, as it can be described as the fluctuation of a photon into a hadronic system which then scatters off the proton. In a previous publication on transverse energy flow, H1 showed that this picture is not only valid in photoproduction but also in DIS [17]. A similar level of $\langle E_T^* \rangle$ in the central pseudorapidity region and a $W$ dependence similar to that observed in hadron-hadron interactions were found. This is consistent with the Bjorken-Kogut picture in which hadronic final state quantities in the central pseudorapidity region are expected to be insensitive to the nature of the colliding particles [13] and depend only on the centre of mass energy.

Fig. 6 shows the $W$ dependence of the new H1 high $Q^2$ data in the central pseudorapidity region ($|\eta^*| < 0.5$) together with our previously published low $Q^2$ results. Data from $p\bar{p}$ and $pp$ experiments [1, 66], taken with non-single diffractive triggers, are also shown. This trigger requirement excludes elastic and quasi-elastic scattering events.

A $W$ dependence compatible with that of the hadron-hadron data is found in the H1 data although the mean transverse energy is larger at high $Q^2$. For a given value of $Q^2$, the increase in $\langle E_T^* \rangle$ seen in the H1 data is consistent with a linear dependence on $\ln W$.

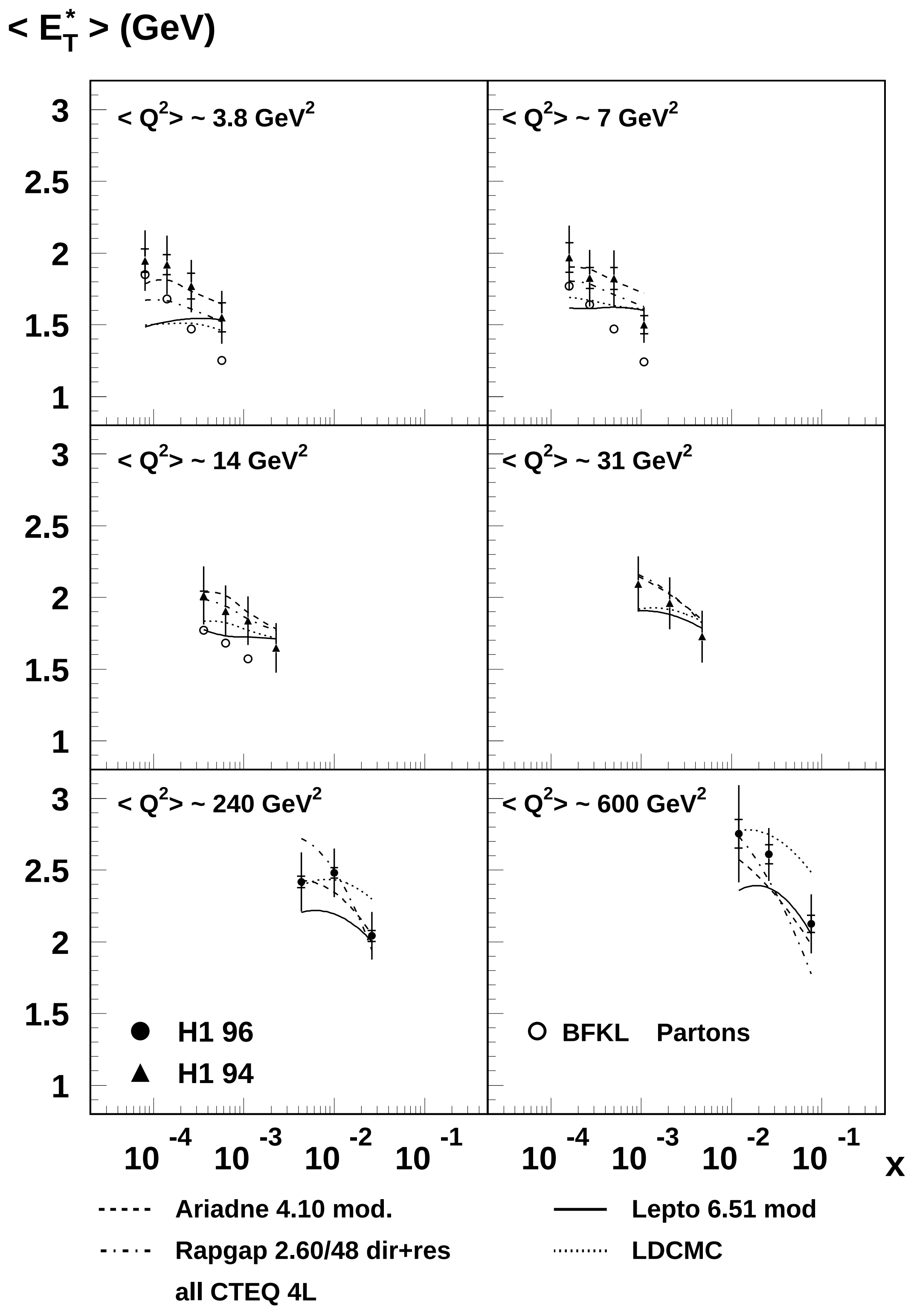


Figure 5: Variation of mean $E_T^*$ in the central pseudorapidity region ($-0.5 < \eta^* < 0.5$) with $x$ in different regions of $Q^2$ compared to four QCD based models and an analytical BFKL calculation.

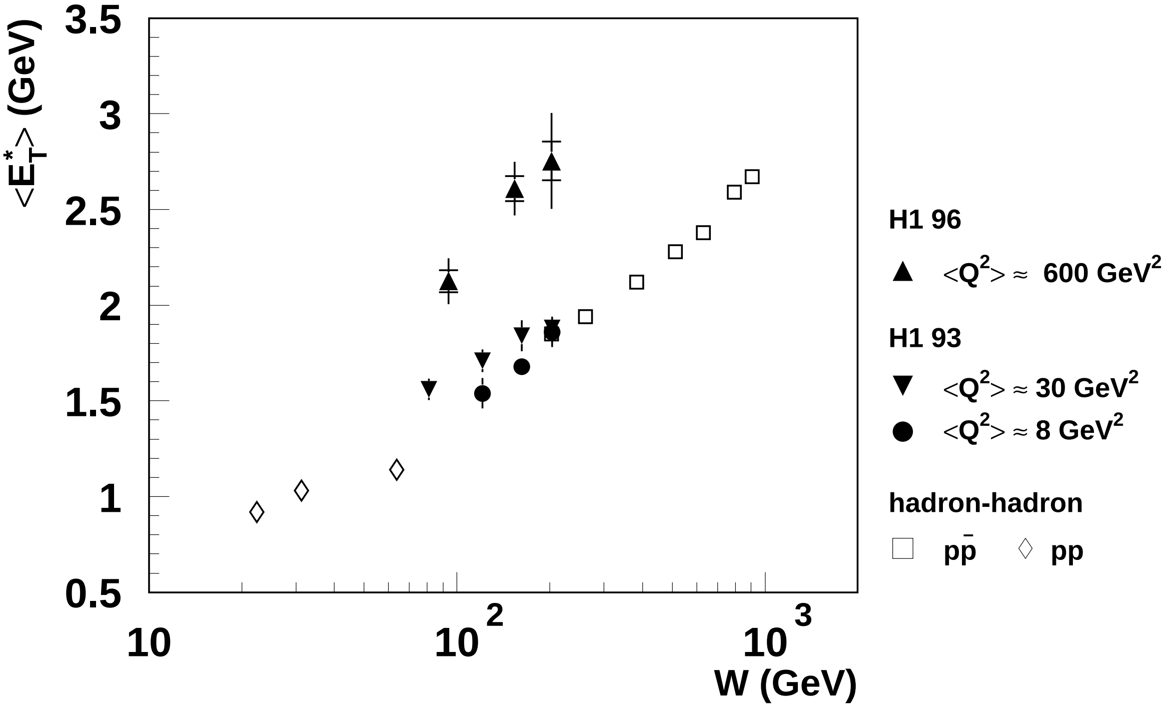


Figure 6: Variation of the average $E_T^*$ in the central pseudorapidity region ($-0.5 < \eta^* < 0.5$) with $W$. The present high $Q^2$ data are shown together with earlier H1 results at lower $Q^2$. Also shown are hadron-hadron results ($p\bar{p}$ and $pp$ from UA1, NA22 and AFS).

In order to investigate further the $Q^2$ dependence, data have been selected from a small range in $W$ ($165$ GeV $< W < 213$ GeV). To ensure consistency with the previous study [17], the $E_{fwd}$ cut is removed for this part of the analysis and data points and model predictions in all subsequent plots are shown with this condition dropped. This has an effect of, at most, 10% for the lowest $Q^2$ points and is negligible for the high $Q^2$ measurements. These fixed-$W$ transverse energy flow measurements are shown in Fig. 7. From these distributions, it can be seen that the maximum of the $E_T$ flow not only increases with $Q^2$ but also that its position moves towards the central pseudorapidity region.

To study the $E_T^*$ flow from the fragmenting photon and in the central pseudorapidity region, two slices in $\eta^*$ are studied, namely the central bin ($-0.5 < \eta^* < 0.5$) and the so-called photon fragmentation bin ($2 < \eta^* < 3$). These are delineated in Fig. 7. The definition of the photon fragmentation bin is somewhat arbitrary. The chosen bin in $\eta^*$ is expected to be dominated by the fragmentation of the hadronic fluctuation of the photon. Since the rapidity range within which particles of mass $m$ can be produced is limited to $\pm \ln W/m$, and the width of the photon fragmentation peak is $\sim \ln(Q^2/m^2)$ [13], the peak position of the transverse energy flow associated with the fragmenting photon moves towards the central pseudorapidity bin as $Q^2$ increases for fixed $W$. This can be seen in Fig. 7.

Fig. 8 shows that the measured transverse energy in the photon fragmentation bin rises with $Q^2$. Qualitatively, this is consistent with the Generalised Vector Dominance Model [67, 68, 69], in which mesons with higher masses can contribute to the scattering at higher $Q^2$. A more

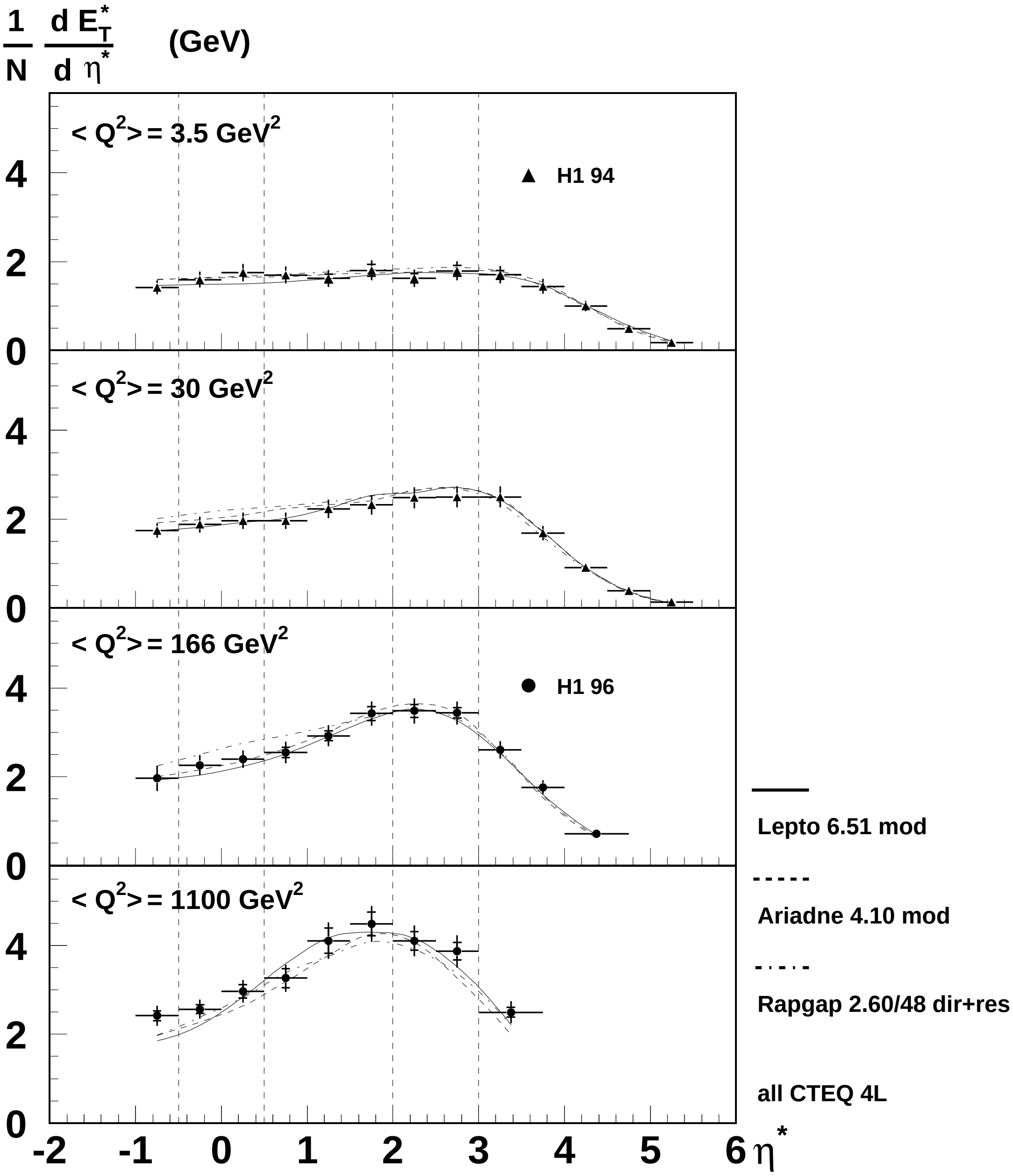


Figure 7: The inclusive transverse energy flow $1/N dE_T^*/d\eta^*$ in different regions of $Q^2$ for $\langle W \rangle \approx$ 185 GeV. The data are compared to three QCD based models. The two pairs of dashed vertical lines denote the central ($-0.5 < \eta^* < 0.5$) and photon fragmentation ($2 < \eta^* < 3$) bins.

formal approach [70] has shown that the photon wave function allows for $q\bar{q}$ states with higher $p_T$ at higher $Q^2$.

Fig. 8 also provides the first experimental evidence for a rise in the transverse energy with $Q^2$ in the central pseudorapidity bin. This result was not observed in previous work [17], which used less than one tenth of the data available for this analysis and which showed no significant $Q^2$ dependence in this region.

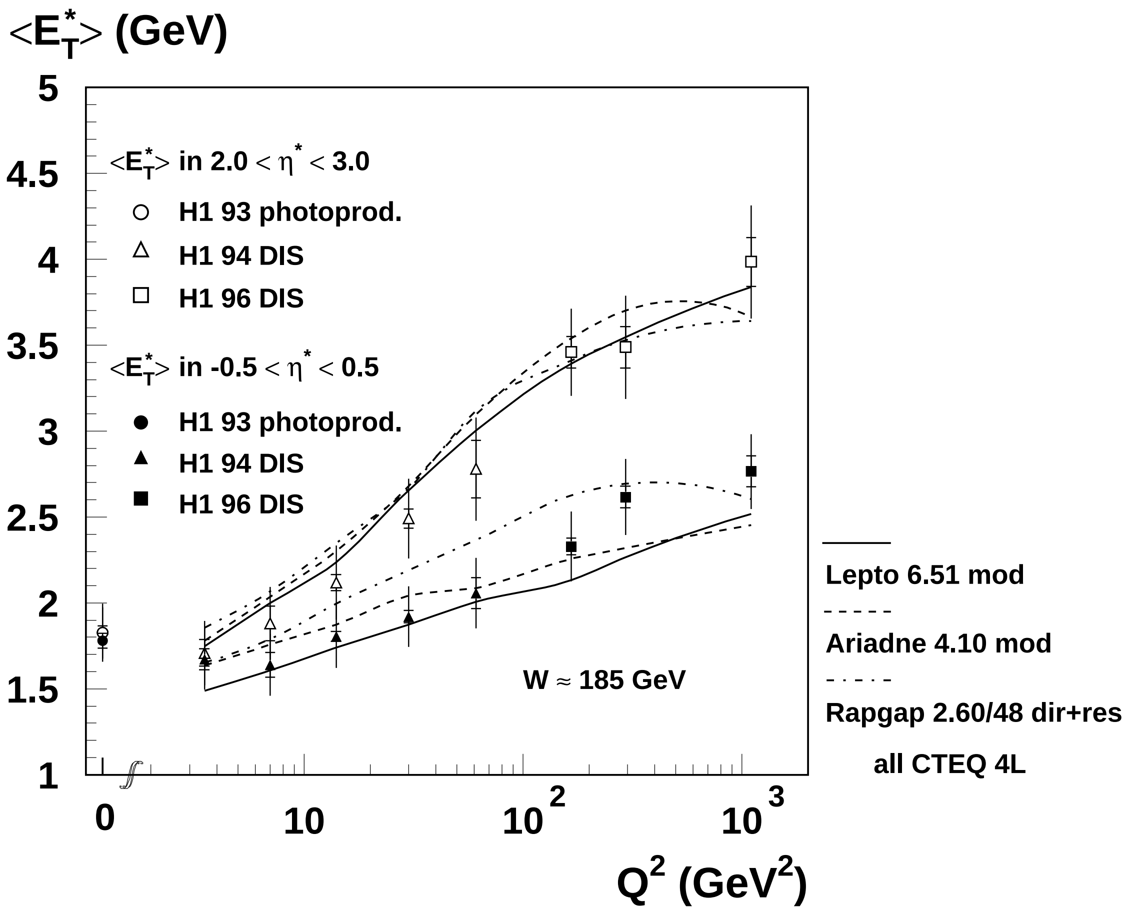


Figure 8: Variation of the mean $E_T^*$ in the central pseudorapidity bin ($-0.5 < \eta^* < 0.5$) and the photon fragmentation bin ($2 < \eta^* < 3$) with $Q^2$. The data are compared to three QCD based models.

Comparisons are made with ARIADNE, LEPTO and RAPGAP. As they are used here, LEPTO and RAPGAP do not include diffractive events. Therefore, the predictions of these models are expected to lie above the data in Fig. 8. However, as the fraction of diffractive events is less than $10\%$, with an average transverse energy production of about one half of that observed in non-diffractive interactions [71], the bias is not larger than $10\%$. A comparison of RAPGAP predictions including pomeron exchange processes with those RAPGAP calculations shown here also supports this. All of the QCD based models describe the rise with $Q^2$ of the measured average transverse energy in the central and photon fragmentation regions although RAPGAP predicts too much transverse energy in the central pseudorapidity range.

## Summary

Measurements of energy production transverse to the photon and proton directions in the hadronic centre of mass system have been presented using deep-inelastic scattering data taken in positron-proton collisions by the H1 Collaboration at HERA. The measurements cover more than 8 units of pseudorapidity and extend over the kinematic range $3.2 < Q^2 < 2\,200$ GeV$^2$, $x > 8 \cdot 10^{-5}$ and $66 < W < 233$ GeV.

For $Q^2$ values below about 10 GeV$^2$ the inclusive transverse energy flow $1/N dE_T^*/d\eta^*$ shows a plateau-like behaviour in the current hemisphere with typical values of about 2 GeV. As $Q^2$ increases, the distribution shows a peak of increasing magnitude. For values of $Q^2$ greater than approximately 70 GeV$^2$, the peak position coincides with the origin of the Breit frame. Transverse energy flow in the vicinity of the proton remnant is observed to be approximately half of that in the current hemisphere, albeit with large systematic uncertainties.

Transverse energy production in the central pseudorapidity region rises with increasing $W$ which is consistent with observations made in hadron-hadron experiments. However, for the first time there is evidence of an increase in the level of transverse energy in the central rapidity region with $Q^2$.

Four QCD based models have been compared to the data. At low $x$ and $Q^2$, predictions made using approaches based on DGLAP and CCFM evolution, implemented within the LEPTO and LDCMC models, respectively, are not able to fully describe the transverse energy flow in the central pseudorapidity region. RAPGAP, which includes resolved virtual photon processes, and the Colour Dipole Model, as implemented in ARIADNE, give a reasonable description of the data in this region. Furthermore, the LEPTO model can only describe the measurements over the full current hemisphere at low $Q^2$ if a General Area Law based string reinteractions scheme is not used. At the highest $Q^2$ values, all models describe the data well except for HERWIG which provides a relatively poor description over most of the kinematic range considered in this analysis.


## Acknowledgements

We are grateful to the HERA machine group whose outstanding efforts have made and continue to make this experiment possible. We thank the engineers and technicians for their work constructing and maintaining the H1 detector, our funding agencies for financial support, the DESY technical staff for continual assistance and the DESY directorate for the hospitality which they extend to the non-DESY members of the collaboration.

# References


[1] UA1 Collaboration, C. Albajar et al., Nucl. Phys. B 335 (1990) 261.

[2] H1 Collaboration, I. Abt et al., Z. Phys. C 63 (1994) 377.

[3] H1 Collaboration, C. Adloff et al., Nucl. Phys. B 485 (1997) 3.

[4] H1 Collaboration, C. Adloff et al., Nucl. Phys. B 497 (1997) 3.

[5] ZEUS Collaboration, J. Breitweg et al., Eur. Phys. J. C 7 (1999) 609.

[6] Yu. L. Dokshitzer, Sov. Phys. JETP 46 (1977) 641;
V. N. Gribov and L. N. Lipatov, Sov. J. Nucl. Phys. 15 (1972) 438 and 675;
G. Altarelli and G. Parisi, Nucl. Phys. 126 (1977) 297. 126 (1977).

[7] E. A. Kuraev, L. N. Lipatov and V. S. Fadin, Sov. Phys. JETP 45 (1972) 199;
Y. Y. Balitsky and L. N. Lipatov, Sov. J. Nucl. Phys. 28 (1978) 822.

[8] M. Ciafaloni, Nucl. Phys. B 296 (1987) 249;
S. Catani, F. Fiorani and G. Marchesini, Phys. Lett. B 234 (1990) 339, Nucl. Phys. B 336 (1990) 18.

[9] H1 Collaboration, S. Aid et al., Phys. Lett. B 356 (1995) 118.

[10] H1 Collaboration, C. Adloff et al., Phys. Lett. B 415 (1997) 418.

[11] ZEUS Collaboration, J. Breitweg et al., Eur. Phys. J. C 6 (1999) 239.

[12] H1 Collaboration, C. Adloff et al., Nucl. Phys. B 538 (1999) 3.

[13] J.D. Bjorken and J.B. Kogut, Phys. Rev. D 8 (1973) 1341.

[14] V. Del Duca et al., Phys. Rev. D 46 (1992) 931.

[15] G. Shaw, Phys. Lett. B 318 (1993) 221;
G. Kerley and G. Shaw, Phys. Rev. D 56 (1997) 7291.

[16] B. I. Ioffe, Phys. Lett. B 30 (1969) 123.

[17] H1 Collaboration, S. Aid et al., Phys. Lett. B 358 (1995) 412.

[18] NA22 Collaboration, M. Adamus et al., Z. Phys. C 39 (1988) 311.

[19] H1 Collaboration, I. Abt et al., Nucl. Instr. and Meth. A 386 (1997) 310 and 348.

[20] H1 Calorimeter Group, B. Andrieu et al., Nucl. Instr. and Meth. A 336 (1993) 460.

[21] H1 Calorimeter Group, B. Andrieu et al., Nucl. Instr. and Meth. A 350 (1994) 57.

[22] H1 Calorimeter Group, B. Andrieu et al., Nucl. Instr. and Meth. A 336 (1993) 499.

[23] J. Ban et al., Nucl. Instr. and Meth. A 372 (1996) 399.

[24] H1 Collaboration, S. Aid et al., Nucl. Phys. B 470 (1996) 3.

[25] H1 SPACAL Group, R. D. Appuhn et al., Nucl. Instr. and Meth. A 382 (1996) 395

[26] A. Meyer, DESY internal report FH1-97-01, 1997.

[27] E. Panaro, DESY-THESIS-1998-020, 1998.

[28] F. Jacquet and A. Blondel in Proc. of the Study of an ep Facility for Europe, ed. U. Amaldi, DESY-79-48, p.391 (1979).

[29] U. Bassler and G. Bernardi, Nucl. Instr. and Meth. A 361 (1995) 197.

[30] G. A. Schuler and H. Spiesberger, Proc. of the HERA Workshop, eds W. Buchmüller and G. Ingelman (1992) Vol. 3, 1419.

[31] M.F. Hess, Ph.D. thesis, Hamburg 1996, MPI-PhE/96-16.

[32] L. Lönnblad, Comp. Phys. Comm. 71 (1992) 15.

[33] G. Marchesini et al., Comp. Phys. Comm. 67 (1993) 465.

[34] G. Ingelman, Proc. of the HERA workshop, eds W. Buchmüller and G. Ingelman, Hamburg (1992) Vol. 3, 1366.

[35] M. Glück, E. Reya and A. Vogt, Z. Phys. C 67 (1995) 433.

[36] A.D. Martin, R.G. Roberts and W.J. Stirling , MRS Parton Distributions, Proc. of the Workshop on Quantum Field Theory Theoretical Aspects of High Energy Physics, eds. B. Geyser and E.M. Ilgenfritz, p.11 (1993).

[37] H. Fesefeldt, The Simulation of Hadronic Showers - Physics and Applications, RWTH Aachen, PITHA 85/02 (1985).

[38] H. Bertini, Phys. Rev. 188 (1969) 1711.

[39] R. Engel, Proc. of the XXIXth Rencontre de Moriond (1994) 321.

[40] M. Dasgupta and B.R. Webber, Eur. Phys. J. C 1 (1998) 539;
H1 Collaboration, C. Adloff et al., Phys. Lett. B 406 (1997) 256.

[41] Yu.L. Dokshitzer, et al., "Basics of Perturbative QCD", Editions Frontieres (1991);
Ya.I. Azimove, Yu.L. Dokshitzer, V.A. Khoze and S.J. Troyan, Z. Phys. C 31 (1986) 213, Z. Phys. C 27 (1985) 65;
L.V. Gribov, Yu.L. Dokshitzer, V.A. Khoze and S.J. Troyan, Phys. Lett. B 202 (1988) 276.

[42] S.R. Sharpe, Proceedings of 29th International Conference on High Energy Physics (ICHEP 98), Vancouver, Canada, July 1998, hep-lat/9811006.

[43] P. Nadolsky, D. R. Stump and C. P. Yuan, MSUHEP-90601, June 1999, hep-ph/9906280.

[44] CTEQ Collaboration, Phys. Rev. D 55 (1997) 1280.

[45] H. Plothow-Besch, PDFLIB Version 7.09, User's Manual, W5051 1997.07.2 CERN-PPE, 1997.

[46] G. Schuler and T. Sjöstrand, Phys. Lett. B 376 (1996) 193.

[47] B. Andersson, G. Gustafson and L. Lönnblad, Nucl. Phys. B 339 (1990) 393.

[48] L. Lönnblad, Z. Phys. C65 (1995) 285;
A. H. Mueller, Nucl. Phys. B415 (1994) 373;
L. Lönnblad, Z. Phys. C70 (1996) 107.

[49] B. Andersson, et al., Nucl. Phys. B 463 (1996) 217;
B. Andersson, et al., Z. Phys. C 71 (1996) 613.

[50] B. Andersson et al., Phys. Rep. 97 (1983) 31.

[51] B.R. Webber, Nucl. Phys. B 238 (1984) 492.

[52] L. Lönnblad, private communication.

[53] N. Brook et al., in Proc. of the Workshop Future Physics at HERA, eds. G. Ingelman, A. De Roeck and R. Klanner, DESY (1996) Vol. 1, 613.

[54] H. Kharraziha and L. Lönnblad, The Linked Dipole Chain Monte Carlo, preprint LU-TH 97-21, NORDITA-97/54 P, hep-ph/9709424, December 1997.

[55] A. Edin, G. Ingelman, J. Rathsman, Phys. Lett. B 366 (1996) 371.

[56] ZEUS Collaboration, J. Breitweg et al., DESY-99-041, accepted by Eur. Phys. J. C (1999) .

[57] J. Rathsman, Phys. Lett. B 452 (1999) 364.

[58] H. Jung, Comp. Phys. Comm. 86 (1995) 147.
(for update see http://www-h1.desy.de/~jung/rapgap/rapgap.html).

[59] T. Sjöstrand, Comp. Phys. Comm. 82 (1994) 74.

[60] M. Seymour, Lund preprint LU-TP-94-12 (1994);
M. Seymour, Nucl. Phys. B 436 (1995) 443.

[61] K. Golec-Biernat et al., Phys. Lett. B 335 (1994) 220 ;
P. Sutton private communication.

[62] H1 Collaboration, C. Adloff et al., Z. Phys. C 76 (1997) 613.

[63] ZEUS Collaboration, J. Breitweg et al., Eur. Phys. J. C 6 (1999) 43.

[64] Yu. L. Dokshitzer, Plenary talk at Int. Workshop on Deep Inelastic Scattering and Related Subjects, Eilat Feb. 1994 (unpublished);
V. A. Khoze and W. Ochs, Int. J. Mod. Phys. A 12 (1997) 2949.

[65] A. H. Mueller, Nucl. Phys. B (Proc. Suppl.) 18C (1990) 125;
A. H. Mueller J. Phys. G17 (1991) 1443.

[66] A. De Roeck, Inclusive Particle Production in Hadron-Proton Interactions at 250 GeV/c, Ph.D. Thesis, Antwerpen 1988.

[67] A. Donnachie and G. Shaw, in Electromagnetic Interactions of Hadrons, Vol. 2, 169-194, eds. A. Donnachie and G. Shaw, Plenum, New York, 1978.

[68] J. J. Sakurai and D. Schildknecht, Phys. Lett. B 40 (1972) 121.

[69] B. Gorczyca and D. Schildknecht, Phys. Lett. B 47 (1973) 71.

[70] S. Brodsky et al., Phys. Rev. D 50 (1994) 3134;
S. Brodsky and P. Lepage, Phys. Rev. D 22 (1980) 2157.

[71] H1 Collaboration, S. Aid et al., Z. Phys. C 70 (1996) 609.